Journal of Neuro-Oncology (2022) 156:109–122
https://doi.org/10.1007/s11060-021-03887-4

LABORATORY INVESTIGATION

Profiling of the immune landscape in murine glioblastoma following blood brain/tumor barrier disruption with MR image-guided focused ultrasound

Natasha D. Sheybani[1] · Alexandra R. Witter[2] · William J. Garrison[1] · G. Wilson Miller[3] · Richard J. Price[1,3] · Timothy N. J. Bullock[2]

Received: 12 August 2021 / Accepted: 26 October 2021 / Published online: 3 November 2021

Abstract

Purpose Glioblastoma (GB) poses formidable challenges to systemic immunotherapy approaches owing to the paucity of immune infiltration and presence of the blood brain/tumor barriers (BBB/BTB). We hypothesize that BBB/BTB disruption (BBB/BTB-D) with focused ultrasound (FUS) and microbubbles (MB) increases immune infiltration in GB. As a prelude to rational combination of FUS with ITx, we herein investigate the impact of localized BBB/BTB-D on innate and adaptive immune responses in an orthotopic murine GB model.

Methods Mice with GL261 gliomas received i.v. MB and underwent FUS BBB/BTB-D (1.1 MHz, 0.5 Hz pulse repetition frequency, 10 ms bursts, 0.4–0.6 MPa). Brains, meninges, and peripheral lymphoid organs were excised and examined by flow cytometry 1–2 weeks following FUS.

Results The number of dendritic cells (DC) was significantly elevated in GL261 tumors and draining cervical LN in response to sonication. CD86 + DC frequency was also upregulated with 0.6 MPa FUS, suggesting increased maturity. While FUS did not significantly alter CD8 + T cell frequency across evaluated organs, these cells upregulated checkpoint molecules at 1 week post-FUS, suggesting increased activation. By 2 weeks post-FUS, we noted emergence of adaptive resistance mechanisms, including upregulation of TIGIT on CD4 + T cells and CD155 on non-immune tumor and stromal cells.

Conclusions FUS BBB/BTB-D exerts mild, transient inflammatory effects in gliomas—suggesting that its combination with adjunct therapeutic strategies targeting adaptive resistance may improve outcomes. The potential for FUS-mediated BBB/BTB-D to modify immunological signatures is a timely and important consideration for ongoing clinical trials investigating this regimen in GB.

Keywords Focused ultrasound · Image guidance · Glioblastoma · Blood brain barrier · Immune · Immunotherapy

Background

Glioblastoma (GB) is the most common and aggressive primary brain malignancy in adults. Even when treated with the standard of care (surgical debulking, radiotherapy, and chemotherapy), its diffuse nature and proclivity for recurrence render it largely intractable. Thus, patients face a dismal prognosis, with a high probability of recurrence (> 90%) and survival on the order of months [1, 2].

Growing evidence refutes historic dogma purporting that the central nervous system (CNS) is a site of immune privilege. This paradigm shift toward consideration of the CNS as "immune distinct" has largely been driven by recent demonstration of a lymphatic system within the CNS [3] and documentation of complex immunological interactions

✉ Natasha D. Sheybani
nds3sa@virginia.edu

✉ Richard J. Price
rprice@virginia.edu

✉ Timothy N. J. Bullock
tb5v@virginia.edu

[1] Department of Biomedical Engineering, Health System, University of Virginia, Box 800759, Charlottesville, VA 22908, USA

[2] Department of Pathology, Health System, University of Virginia, Box 801386, Charlottesville, VA 22908, USA

[3] Department of Radiology and Medical Imaging, Health System, University of Virginia, Charlottesville, VA, USA

between the CNS and periphery [4]. These advances have underscored growing interest in evaluation of immunotherapy approaches in brain tumors, including GB [5–7]. Despite some encouraging early stage and anecdotal results, advanced clinical trials assessing single-agent immunotherapies GB have largely been negative owing to factors such as poor pre-existing lymphocytic infiltration, complex adaptive mechanisms of immunosuppression and protection of tumor cells by the blood brain/blood tumor barrier (BBB/BTB) [8, 9].

Consequently, there exists a critical—yet unmet—demand for adjunct approaches designed to bolster effector immune cell infiltration, curb mechanisms of immunosuppression in GB and surmount the challenges to systemic drug delivery imposed by the BBB/BTB. GBTo this end, this study investigates BBB/BTB disruption (BBB/BTB-D) with MR imaging-guided focused ultrasound (FUS) and microbubbles (MB) as an approach for modulating anti-tumor immunity in a preclinical model of GB. FUS + MB has been demonstrated as a safe, non-invasive, non-ionizing technique for transient, localized, and reversible BBB/BTB permeabilization. The extracorporeal nature of this technology obviates the need for invasive intracranial catheterization, injection or implantation. FUS BBB/BTB-D has been demonstrated to improve the delivery of chemotherapies [10–13], antibodies [14–18], cytokines [19] and immune cells [20, 21] to brain malignancies. More recently, FUS BBB disruption has been demonstrated to invoke sterile inflammation in the brain including acute changes to trophic factors, alarmins, cytokines and chemokines [22–26]. While such effects are not necessarily desirable in normal brain tissue or neurological pathologies with an existing chronic inflammation component, the concept of FUS-mediated immune modulation is of great interest in the setting of brain malignancies including GB, wherein anti-tumor inflammation may be favorable [27, 28]. That said, studies have shown that such parameters as MB formulation and dose [23, 29], anesthesia protocol [26, 30, 31] and number of BBB opening sessions [29] can differentially impact inflammatory response to FUS, and despite recent work having demonstrated that FUS BBB/BTB-D can promote the efficacy of immunotherapies in GB [18, 32], the influence of the aforementioned parameters on GB immunobiology following this regimen is yet unresolved.

Clinical investigation of FUS BBB and/or BTB opening has been burgeoning over the last 5 years. Safety and feasibility have been confirmed across multiple pathologies including GB [33–35], ALS [36] and Alzheimer's disease [37, 38]. In addition to these pathologies, FUS-mediated barrier disruption is currently being evaluated in Parkinson's disease dementia (NCT03608553), low grade glioma (NCT04063514) and HER-2 + breast cancer brain metastases (NCT03714243). A first-in-human trial combining FUS with immunotherapy in brain malignancies will soon assess the safety and efficacy of nivolumab and BBB/BTB-D in melanoma brain metastases (NCT04021420).

Motivated by the tremendous potential of FUS to potentiate immunotherapeutic agents in GB, this study is founded upon the need for systematic characterization of GB immunobiology following FUS BBB/BTB-D, as well as filling the existing gap in our understanding of how FUS exposure conditions influence this immunobiology. We here report on the impact of two distinct FUS peak negative pressures (0.4 and 0.6 MPa) on elaboration of local and systemic immune responses 1–2 weeks following FUS BBB/BTB-D in orthotopic GL261 tumors. These findings generate important considerations for pre-clinical investigations of FUS immunotherapy in brain tumors as well as timely insights for clinical trials seeking to deploy FUS BBB/BTB-D in GB.

Methods

Cell line and culture

Luciferase-transduced GL261 cells (GL261-luc2) obtained from the Woodworth Lab (University of Maryland) were cultured in high glucose 1 × Dulbecco modified Eagle medium (DMEM, Gibco) supplemented with 1 mM sodium pyruvate (Gibco), non-essential amino acids (Gibco), 10% fetal bovine serum (Gibco), and 100 ug/ml G418 (GoldBio). Cells were maintained at 37 °C and 5% CO_2. Thawed cells were cultured for up to three passages and maintained in logarithmic growth phase for all experiments. Cells tested negative for mycoplasma.

Intracranial tumor cell inoculation

GL261-luc2 cells (1×10^5 cells per 2 µl) were resuspended in sterile PBS for intracranial tumor implantation. Cells were implanted into the right striatum of 6–10 weeks female C57BL/6 mice (The Jackson Laboratory). Following anesthetization with an intraperitoneal injection of ketamine (50 mg/kg; Zoetis) and dexdomitor (0.25 mg/kg; Pfizer) in sterilized 0.9% saline, the heads of mice were depilated, aseptically prepared, and placed into a stereotactic head frame. Cells were implanted at a mechanically controlled rate of 0.5 µl/min using a Hamilton syringe and micropump (UltraMicroPump, World Precision Instruments). Injection coordinates were ~ 2.0 mm lateral from the sagittal suture, 0.5 mm anterior of bregma and 3 mm below the dura. Mice were housed on a 12/12 h light/dark cycle and supplied food ad libitum. Animal experiments were approved by the Animal Care and Use Committee at the University of Virginia and conformed to the National Institutes of Health guidelines for the use of animals in research.

MRI-guided focused ultrasound for BBB/BTB-D

Two weeks following brain tumor inoculation, mice were anesthetized with an intraperitoneal injection of ketamine (50 mg/kg; Zoetis) and dexdomitor (0.25 mg/kg; Pfizer) in sterilized 0.9% saline. Tails were cannulated to allow for intravenous (i.v.) injections of MRI contrast agent and MB. Mouse heads were shaved and depilated in preparation for MRI-guided focused ultrasound treatment. Each mouse was positioned supine on a custom surface transmit-receive RF coil (to maximize imaging SNR) with the head coupled to a 1.14 MHz spherical single-element transducer via degassed water bath housed within an MR-compatible FUS system (RK-100; FUS Instruments). Image-guidance was enabled by co-registration of FUS system coordinates to those of the 3 T MRI (Prisma, Siemens) within which the system was placed for studies. MRI contrast agent (0.05 ml of 105.8 mg/ml preparation; MultiHance Bracco Diagnostic Inc.) was administered i.v. to confirm tumor location by contrast-enhanced MR imaging. A four-spot grid of sonications was overlaid on the MR-visible tumor and sonications were carried out at a 0.5% duty cycle for 2 min. All sonications were performed at a non-derated peak negative pressure of either 0.4 or 0.6 MPa, in the presence of i.v. injected albumin-shelled MB (1×10^5/g B.W.). MB were fabricated in-house and characterized as previously described [39, 40]. Contrast-enhanced MR imaging was repeated to confirm BBB/BTB-D. Following FUS exposure, mice were moved to a heating pad for recovery. Mice were given Antisedan subcutaneously for anesthesia reversal. MRI parameters and passive cavitation detection (PCD) methods detailed in Supplemental Information (SI).

Flow cytometry

Immunological characterization was conducted on samples obtained from euthanized, tumor-bearing mice at 21 and 28 days post-inoculation. In order to gain resolution into tissue resident versus vascular immune cell populations, mice were i.v. injected with a fluorescently conjugated αCD45 antibody ~ 2 min prior to euthanasia. Whole brains were excised in order to preserve the entirety of the tumor as well as its infiltrative margins. Additionally, spleens, cardiac blood, superficial cervical lymph nodes, deep cervical lymph nodes and meninges were harvested, following which all samples were processed for flow cytometry. Detailed methods for sample processing and staining are described in SI. To gauge cytokine expression in T cells, samples were stimulated with either plate bound (5 µg/ml) αCD3 or PMA (0.2 ug/ml:ionomycin (4 uM) for 4 h in the presence of brefeldin-A (10 µg/ml). Surface staining was performed followed by fixation and permeabilization in order to stain for IFNγ or Granzyme B. Unstimulated cells were used as baseline controls for cytokine production. Samples were run on either the CytoFLEX flow cytometer (Beckman Coulter) or Attune NxT flow cytometer (Thermo Fisher Scientific). Data analysis was conducted using FlowJo (Treestar) or FCSExpress (DeNovo).

Interferon-gamma assay

Supernatants from homogenized whole brains of naïve mice, untreated or treated GL261-luc2 tumor-bearing mice were assayed for immunocytokine representation using the Mouse IFN-gamma DuoSet ELISA kit (R&D Systems #DY485-05, #DY008). This was conducted in accordance with manufacturer's instructions.

Statistical analysis

All statistical analyses were performed in Graphpad Prism 8 and 9 (Graphpad Software, Inc). Unless otherwise noted, flow cytometry data are displayed in normalized format (i.e. fold change over mean of control group). Outliers were removed via Grubb's test. Statistical indicators refer to $*p < 0.05$, $**p < 0.01$ and $***p < 0.001$ vs. group(s) indicated, with numerical p-values noted on figure panels for all $p < 0.2$. Statistical significance was defined as $p < 0.05$. Unpaired Student's t-test was used to determine statistical significance for comparisons of two groups. One-way ANOVA followed by either Dunnett or Tukey multiple comparison correction was utilized for comparisons of three or more groups. Comparison of multiple groups across multiple organs was performed by two-way ANOVA followed by Tukey multiple comparison correction. All values are reported as mean ± standard error of the mean (SEM) unless otherwise noted.

Results

Differential impact of MR-image guided FUS peak negative pressures on BBB/BTB-D in GL261 tumors

An orthotopic glioma model was established via implantation of 100,000 GL261 cells into the right striatum of mice. Two weeks following intracranial tumor implantation, FUS-mediated BBB/BTB-D disruption was performed in a subset of MR-visible GL261 tumors targeted with a 4-spot grid of sonications (1.1 MHz, 0.5% duty cycle) applied at either 0.4 or 0.6 MPa, as measured in water, in the presence of systemically circulating MB. At the conclusion of the 2-min sonication period, contrast-enhanced MR imaging was repeated to verify BBB/BTB-D (Fig. 1A). Quantification of changes in MRI contrast enhancement based on disruption of either GL261 BTB or BBB/BTB revealed no

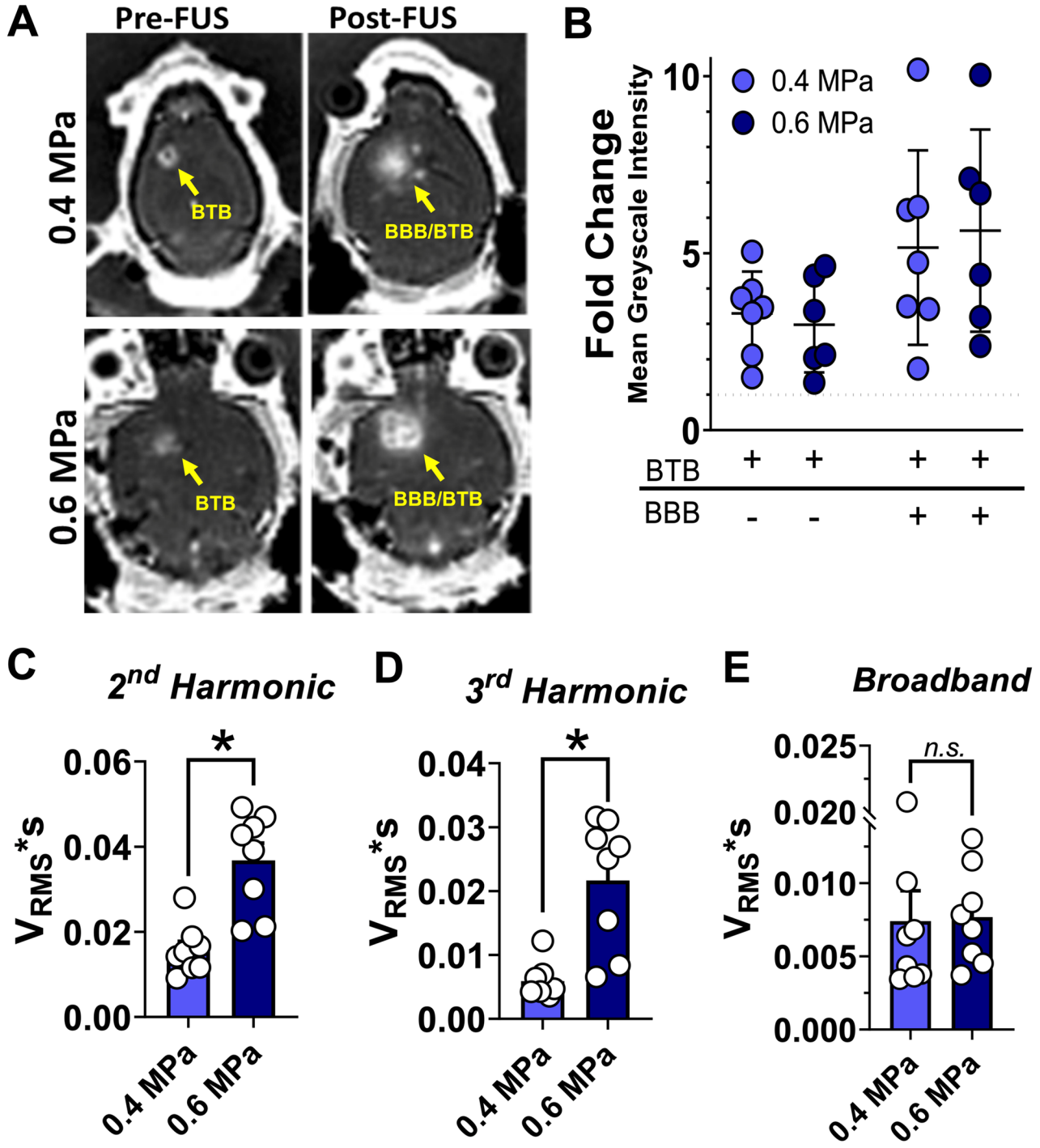

Fig. 1 MR-image guided FUS-mediated blood brain/tumor barrier disruption in GL261 tumors at two peak negative pressures. **A** Representative contrast MR images of GL261 tumor-bearing brain pre- and post-FUS BBB/BTB-D at peak negative pressures of 0.4 and 0.6 MPa. Yellow arrows denote GL261 tumors before and after BBB/BTB-D. **B** Quantification of change in mean greyscale intensity of MR-visible tumors following FUS BBB/BTB-D at 0.4 and 0.6 MPa. ROIs based on BTB and BBB/BTB were separately assessed. Mean ± SD. No significance detected. **C**–**E** Passive cavitation analyses for 2nd harmonic (**C**), 3rd harmonic (**D**) and broadband (**E**) acoustic emissions. n = 6–8 per group. Data reported for one representative experiment. *n.s.* not significant

significant difference across FUS PNP (Fig. 1B). Nonetheless, PCD revealed significant differences in 2nd (Fig. 1C) and 3rd harmonic (Fig. 1D) emissions, consistent with a "dose-dependent" increase in MB oscillations with increasing PNP. Broadband emissions did not differ significantly from 0.4 to 0.6 MPa (Fig. 1E).

Evaluation of innate immune response to FUS BBB/BTB-D in GL261 tumors

In response to the observation from acoustic emissions data that PNPs of 0.4 and 0.6 MPa distinctly confer mechanical energy deposition into GL261 tumors, we performed a series of flow cytometry studies designed to evaluate the differential impact of PNP on immunological response to FUS BBB/BTB-D (Fig. 2A). We first interrogated the impact of FUS BBB/BTB-D on the innate immune response. In order to evaluate the hypothesis that mechanical perturbation of GL261 tumors with FUS + MB can lead to elevated local or peripheral DC representation and maturity, we harvested tumors and secondary lymphoid organs 1 and 2 weeks following FUS for flow cytometry analysis. We observed that 0.6 MPa FUS significantly elevates CD11b + myeloid cell representation in GL261 tumors 1 week following BBB/BTB-D; a 1.7- to 2.3- fold elevation in absolute cell number was noted relative to control and 0.4 MPa FUS tumors, respectively (Figure S1A). Correspondingly, this higher PNP conferred a strong trend toward increased absolute number of intratumoral DCs (Fig. 2B). In the draining cervical LN (DLN), 0.4 MPa FUS significantly elevated the number of DCs by ~ twofold at Day 21 (Fig. 2C). An opposing trend to those in the tumor and LN was observed in the meninges, where DC numbers decreased with increasing FUS PNP (Fig. 2D). This was consistent with the decreasing trend in meningeal CD11b + cell representation invoked by FUS (Fig. S1B). No significant differences in DC percentage were detected in tumors, DLN or meninges at Day 21 (Fig. 2E–G). By Day 28, there were no noteworthy FUS-induced changes in DC numbers or percentages across organs. Moreover, the effects observed 1 week following FUS were not preserved by the 2 week time point (Fig. S2A–F).

We next evaluated expression of CD86—a marker of DC maturity—as a proxy for activation status. CD86 expression was significantly enriched on intratumoral DCs following 0.6 MPa FUS (Fig. 2H). No significant changes in absolute number of CD86 + DCs were noted in the DLN (Fig. 2I) or meninges (Fig. 2J). Moreover, no changes in DC maturation were noted at Day 28 (Fig. S2G–I). Across both timepoints, there were no appreciable changes in percentage of CD86 + DCs (Fig. S3A–F) or CD86 geometric fluorescence intensity (GMF) (Fig. S3G–H), suggesting that the mechanical stimulus invoked by FUS at these PNP was neither sufficient to promote trafficking of mature DCs into tumors, DLN, or meninges, nor to elevate the activation status of DCs already within these sites.

Evaluation of adaptive immune response to FUS BBB/BTB-D in GL261 tumors

Our observation of a modest, yet significant, DC response to FUS BBB/BTB-D in GL261 tumors prompted us to next evaluate whether this translates to changes in local and/or systemic T cell populations. Flow cytometry analysis revealed that intratumoral CD8 + and CD4 + T cells were not significantly altered by FUS at either time point (Fig. 3A, B, E, F). In fact, variable trends in decreasing intratumoral T cell percentage were noted with FUS. Neither FUS PNP elicited significant changes in CD8 + T cells within DLN (Fig. 3C, G) or meninges (Fig. S4A–C), though decreasing trends in meningeal CD8 + T cell representation were noted at both FUS pressures. A significant decrease in CD4 + T cells was observed in DLN 1 week following 0.4 MPa FUS (Fig. 3C). This effect appeared to be transient (Fig. 3H) and was not recapitulated in other tissues (Fig. S4D–F). Aside from changes in T cells, we additionally interrogated B and natural killer (NK) cells. Changes in the representation of these cell types was only noteworthy in the meninges, wherein numbers and percentages exhibited decreasing trends with FUS (Fig. S4G–J).

In order to interrogate T cell activation status, we also evaluated expression of checkpoint molecules, which are commonly expressed after TCR engagement. One week post-FUS, absolute number of PD1-expressing CD8 + T cells in GL261 tumors showed an increasing trend with 0.6 MPa FUS (Fig. 4A), while the corresponding percentage of these cells increased significantly at 0.4 MPa (Fig. 4B). At this time point, trends in TIM3 upregulation were noted following FUS, but not in TIGIT expression (Fig. 4D, E, G, H). Most strikingly, percentage of TIM3-expressing intratumoral CD8 + T cells was significantly elevated following 0.4 MPa FUS, with 0.6 MPa FUS trending in a similar manner (Fig. 4H). These markers remained unchanged on intratumoral CD4 + T cells (data not shown). By Day 28, the noted effects of FUS on checkpoint molecule expression had dissipated (Fig. 4C, F, I).

In the DLN, TIGIT expression on CD4 + T cells displayed a decreasing trend 1 week following FUS (Fig. S5A); notably, this trend reversed at the 2 week time point, wherein FUS generated an increase in TIGIT expression on CD4 + T cells, reaching significance at 0.6 MPa (Fig. S5B).

In tandem with our assessment of checkpoint molecules, we evaluated canonical markers of T cell function including granzyme-B (GzB) and interferon-γ (IFNγ). The percentage of CD8 + T cells expressing these markers was largely unaltered by FUS at both time points (Fig. 5A–D). A similar observation was made in the DLN (Fig. S6). IFNγ GMF

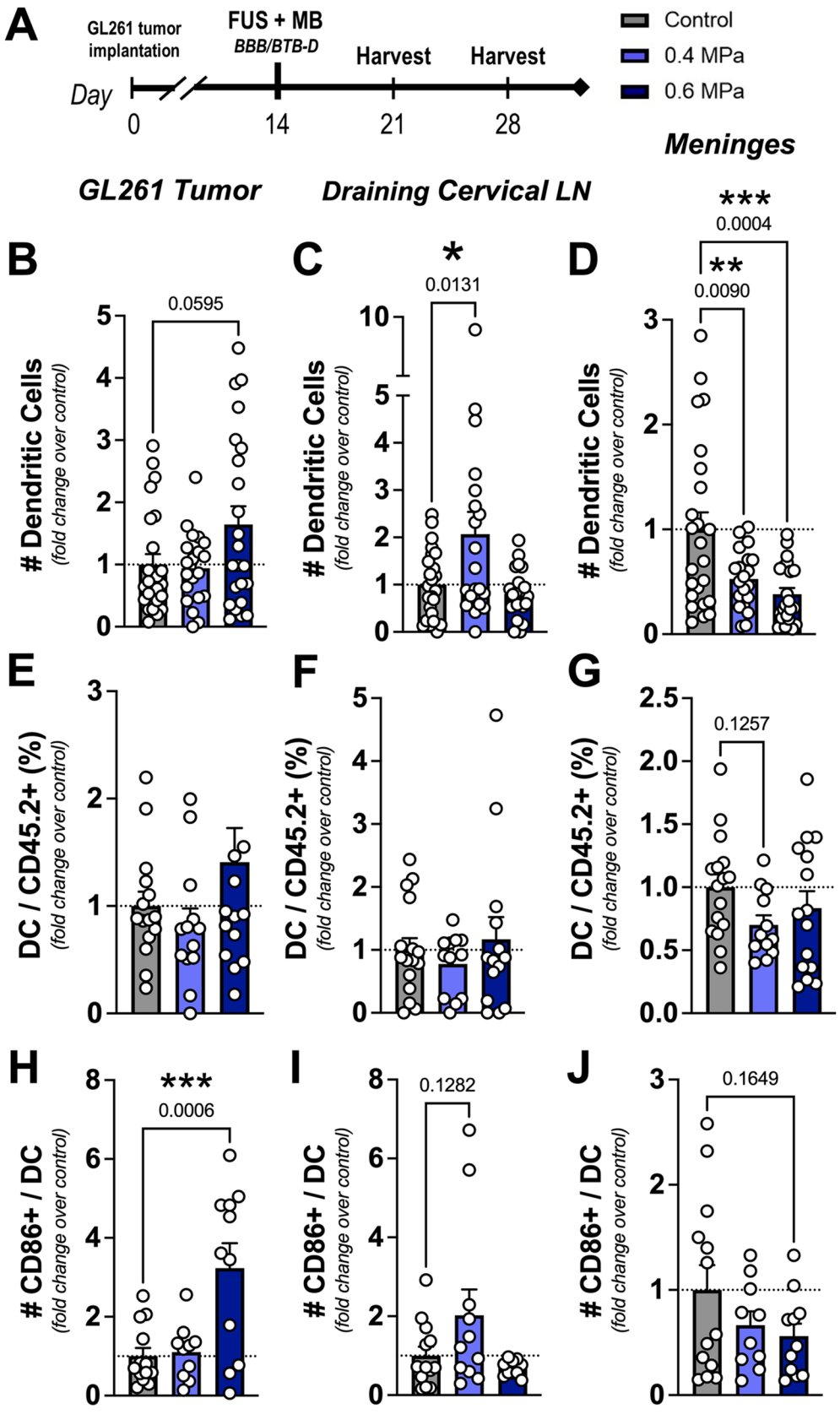
A
GL261 tumor implantation
FUS + MB
BBB/BTB-D
Harvest
Harvest
Day
0
14
21
28
Control
0.4 MPa
0.6 MPa
Meninges
GL261 Tumor
Draining Cervical LN
B
C
D
Dendritic Cells
(fold change over control)
0.0595
*
0.0131
***
0.0004
**
0.0090
E
F
G
DC / CD45.2+ (%)
(fold change over control)
0.1257
H
I
J
CD86+ / DC
(fold change over control)
***
0.0006
0.1282
0.1649

◂**Fig. 2** Dendritic cell representation in tumors, meninges and draining cervical lymph nodes at Day 21 post-implantation. **A** Overview of experimental design. An orthotopic glioma model was established via intracranial implantation of murine GL261 cells. Two weeks following, mice were randomized into three groups (control, 0.4 MPa FUS or 0.6 MPa FUS) and BBB/BTB-D was performed. Tissues were harvested for flow cytometry analysis either 1 or 2 weeks following BBB/BTB-D. **B**–**D** Fold change in absolute number of CD11c-hi, MHC II + dendritic cells in GL261 tumors (**B**), draining cervical lymph nodes (**C**) and meninges (**D**). n = 20–24 per group. Data reported for 4 independent experiments. **E**–**G** Fold change in percentage of CD11c-hi, MHC II + dendritic cells out of CD45.2 + immune cells in GL261 tumors (**E**), draining cervical lymph nodes (**F**) and meninges (**G**). n = 12–16 per group. Data reported for 2 independent experiments. **H**–**J** Fold change in absolute number of CD86 + dendritic cells in GL261 tumors (**H**), draining cervical lymph nodes (**I**) and meninges (**J**). n = 10–13 per group. Data reported for 2 independent experiments

was significantly higher in intratumoral CD8 + T cells as compared with those in meninges or draining LN (Fig. S7A). IFNγ GMF in intratumoral CD8 + T cells also saw increasing trends with FUS at both time points, though this increase did not reach statistical significance (Fig. 5E, G). Consistent with this, a global assessment of IFNγ concentration from whole GL261-bearing brain homogenates revealed no significant influence attributable to FUS (Fig. S7B). While IFNγ GMF remained unchanged on CD4 + cells at Day 21 (Fig. 5I), a significant decrease emerged by Day 28 (Fig. 5K). Neither CD8 + nor CD4 + T cells exhibited significant changes in GzB GMF at the time points assessed (Fig. 5F, H, J, L).

Evaluation of checkpoint ligand expression in GL261 tumors following FUS BBB/BTB-D

During flow cytometry processing, single cell suspensions were divided into CD45.2 + (immune) and CD45.2- (non-immune) cell populations. Within tumor specimens, the latter population was anticipated to be predominantly comprised of GL261 and stromal cells. Both compartments were interrogated for expression of PD-L1 and CD155, the checkpoint ligands that engage with PD1 and TIGIT, respectively. Overall checkpoint ligand expression levels were quite low on CD45.2- cells relative to the much higher expression on their CD45.2 + counterpart. PD-L1 expression on CD45.2- cells was not significantly influenced by FUS at Day 21 or 28 (Fig. S8A, B). One week following BBB/BTB-D, CD155 trended toward decreased expression on CD45.2- cells with increasing FUS PNP (Fig. S8C). Interestingly, this trend reversed at the 2 week time point, with 0.6 MPa FUS conferring a significant upregulation in CD155 expression, nearly twofold over that of control GL261 tumors (Fig. S8D). The percentage of CD45.2- cells dually expressing PD-L1 and CD155 was significantly decreased 1 week following FUS, irrespective of PNP (Fig. S8E); this effect was not preserved on reassessment at Day 28 (Fig. S8F). Checkpoint ligand expression on intratumoral CD45.2 + cells was unaltered by FUS (Fig. S9).

Discussion

BBB disruption via FUS and MB has emerged as a promising and transformative strategy for non-invasive therapy in the CNS. While this technique has been demonstrated to be safe and repeatable across multiple CNS pathologies including GB [34–38], emerging evidence suggests that FUS-mediated disruption of the BBB invokes endogenous neuroinflammatory mechanisms [25, 28, 41, 42]. Indeed, a recent study from our group, using a brain metastasis model of melanoma, demonstrated a mild and transient pro-inflammatory effect of FUS BBB/BTB-D – using acoustic parameters comparable to ours [28]. In contrast with our longitudinal assessments at 1 and 2 weeks post-FUS, our previous study focused on more acute time points in an effort to capture changes in the innate immune compartment. Nonetheless, the observed signatures therein were determined unlikely to elicit a systemic anti-tumor immune response.

In this report, we phenotypically and functionally profile the immunological impact of FUS BBB/BTB-D at two different PNP levels in GL261 glioma-bearing mice. We evaluated the impact of two different PNPs activating Optison-like MB. Prior studies have compared the influence of Optison with other MB formulations for FUS BBB-D [43–45]. Among these other formulations are Definity lipid-shelled MB, the formulation most commonly in use for clinical investigations of FUS BBB-D. While some studies have concluded that Optison and Definity induce similar BBB-D effects and persistence [44], others have shown that Optison may produce a larger effect for a given acoustic pressure amplitude [45]. To our knowledge, no studies to date have performed this type of detailed immunological assessment in primary brain tumors, nor have they evaluated the influence of acoustic exposure conditions on resulting immunobiology. Our study revealed that FUS incites moderate, transitory signatures of innate and adaptive inflammation in response to differing degrees of mechanical energy deposition. Collectively, our findings draw attention to important considerations and opportunities for future pre-clinical studies seeking to advance the role of FUS BBB/BTB-D in immunotherapy.

The PNPs that we chose to evaluate at 1 MHz were previously established to fall within a safe, stable cavitation regime when applied to brain tumors in the presence of circulating MB [13, 46]. We independently evaluated acoustic emissions to confirm that these PNPs indeed confer differential mechanical energy deposition within the targeted focal region. We observed that our chosen

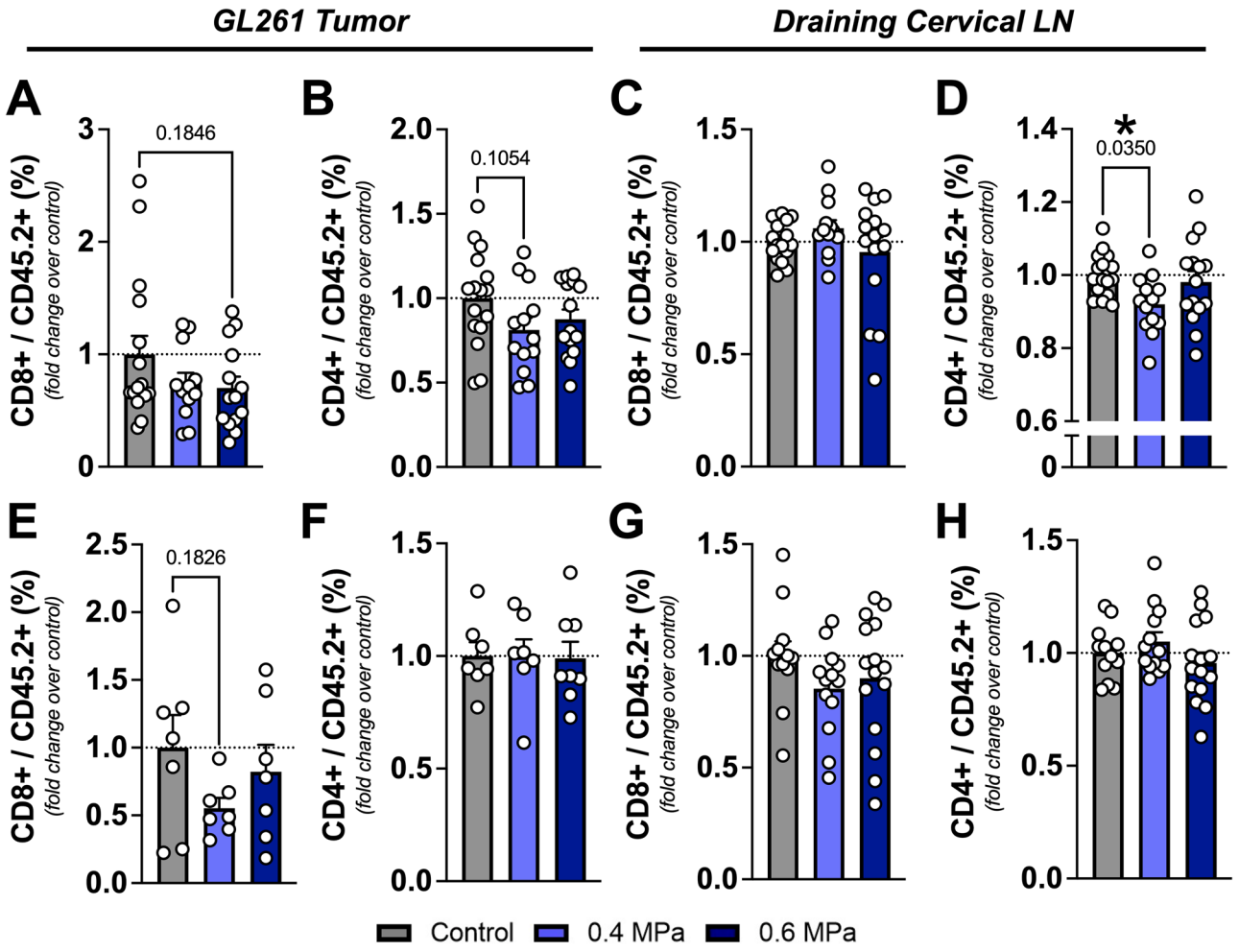

Fig. 3 T cell representation in tumors and draining cervical lymph nodes. **A**–**H** Fold change in percentage of CD8 + and CD4 + T cells out of CD45.2 + immune cells in GL261 tumors (**A**, **B**, **E**, **F**) and draining cervical lymph nodes (**C**, **D**, **G**, **H**) at Days 21 (**A**–**D**) and 28 (**E**–**H**) post-implantation. Day 21 panels: n = 12–16 per group. Data reported for 2 independent experiments. Day 28 panels: n = 7–15 per group. Data reported for 1–2 independent experiments

PNPs conferred an increase in CD11b + myeloid cells 1 week post-FUS; this was accompanied by an inverse trend in the meninges, which mirrored the decreasing trend in overall CD45.2 + immune cells in the meninges as well (Fig. S10A). DCs are a critical antigen-presenting myeloid cell population owing to their ability to initiate and direct adaptive immune responses [47, 48]. We observed that FUS BBB/BTB-D induced elevated DC frequency in GL261 tumors and draining cervical LN, as well as the frequency of CD86 + DC in tumors. Consistent with previous reports, we did not observe changes in the percentage or GMF of CD86-expressing DC in tumors or DLN [28]. As DC percentages in tumors and DLN did not change, but trends in DC numbers did, we postulated that FUS may be increasing the accessibility of the tumor and DLN to the panoply of immune cells. Interrogation of these compartments for fluctuations in overall immune cells revealed that 0.4 MPa FUS indeed elevated CD45.2 + cells in DLN (Fig. S10B), but not in tumors (Fig. S10C).

The trends toward elevation of DC frequency in tumors and DLN were inversely recapitulated in the meninges. Studies in other disease models have shown that accumulation of DCs in the meninges can precede their accumulation in the CNS parenchyma [49]. This is consistent with the hypothesis that the decreasing trends in both overall and CD86 + meningeal DC frequencies, as well as the trend toward reduced DC percentage in the meninges, may have been the compensatory result of DCs trafficking from the meninges to a different site following FUS.

Innate inflammation in the CNS can also be driven by free drainage or trafficking of antigens to secondary lymphoid organs, most prominently the cervical lymph nodes [50, 51]. While 0.4 MPa FUS conferred significant elevation in DC numbers within the draining cervical LN, 0.6 MPa FUS left this population unaltered. These findings are difficult to reconcile, but one possible explanation is that 0.4 MPa FUS may have promoted a better environment for exposure to cytokines and DAMPs capable of regulating DC trafficking to the LN—one that was not recapitulated at the higher PNP.

The changes that FUS mediated in DC frequency and maturity in tumor and LN compartments prompted us to assess de novo T cell responses to GL261 tumors. Our time points were selected with the intent of capturing early and later stages of adaptive immunity. However, across these time points, we did not observe BBB/BTB-D-mediated changes in the magnitude of CD8 + and CD4 + T cell populations within tumors or DLN. Though GL261 tumors were poorly infiltrated by CD8 + T cells, T cell activation was modulated by FUS exposure. Within 1 week of FUS, percentage of PD1 and TIM3 expression on CD8 + T cells saw significant elevation with TIGIT expression trending similarly. As these molecules can reflect either T cell activation or exhaustion, we additionally evaluated T cell function in order to contextualize the impact of FUS on T cells. At this time point, we did not observe changes in functional molecules such as GzB and IFNγ suggesting that the proportion of cytokine-producing cells in the GL261 tumor microenvironment did not increase with FUS.

We also evaluated checkpoint ligand expression within the GL261 tumor microenvironment, specifically PD-L1 and CD155. PD-L1 interacts with PD1 on lymphocytes to attenuate effector T cell responses and enable immune escape [52]. CD155 (also known as poliovirus receptor) serves as the ligand for TIGIT, and its overexpression on tumor cells has been shown to promote tumor cell invasion, migration and ultimately, tumor progression [53]. These molecules are tightly associated in glioma and have been implicated as biomarkers of poor prognosis [54]. At Day 21, consistent with the alleviation of immunosuppressive checkpoint phenotypes on T cells, co-expression of CD155 and PD-L1 on non-immune (CD45.2-) tumor/stromal cells decreased following FUS BBB/BTB-D at both PNPs. CD155 expression trended similarly. By Day 28, FUS-recipient groups saw increased CD155 expression on CD45.2- cells, most prevalently in the 0.6 MPa FUS group. Concordantly, at Day 21, TIGIT expression on CD4 + T cells displayed a decreasing trend in the DLN, which ultimately reversed 1 week later, also reaching significance at 0.6 MPa. Our efforts to contextualize these changes by interrogating T cell function revealed increasing trends in IFNγ GMF on CD8 + T cells. However, neither PNP conferred robust changes in IFNγ expression by CD8 + or CD4 + (data not shown) T cells. Though CD8 + T cells in GL261 tumors had higher IFNγ levels as compared with meninges and draining cervical LN—suggesting a richer abundance of functional T cells at baseline—BBB/BTB-D did not influence this difference. Thus, more detailed assessments of T cell function are needed in future studies.

Our investigation of the impact of PNP on immune response did not delineate a clear differential immune response across pressures. 0.4 MPa FUS was generally noted to confer more favorable anti-tumor stimuli at the 1-week time point. Future investigations should consider the role of immunological adjuvants to elaborate a more robust T cell response with FUS BBB/BTB-D. To this end, our systematic assessment herein has unveiled potential therapeutic targets that may be well suited for delivery with FUS BBB/BTB-D. For example, aligning FUS with inhibitors of the TIGIT/CD155 and/or PD1/PD-L1 axes may be a promising approach. Indeed, a recent study has demonstrated that dual checkpoint blockade with αTIGIT and αPD1 is a promising approach in glioma [55].

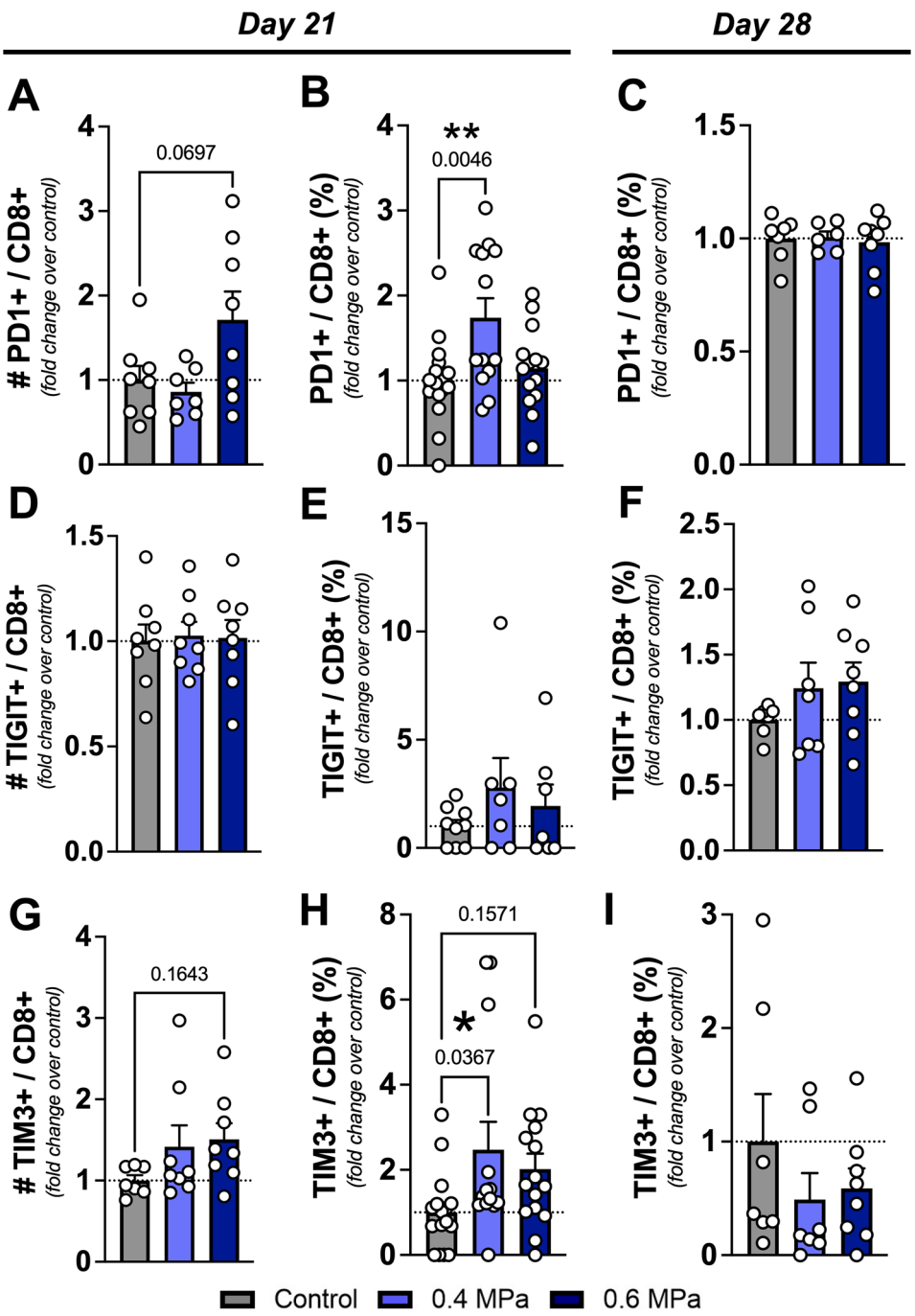

Fig. 4 Checkpoint molecule expression on intratumoral CD8 + T cells. **A**–**C** Fold change in absolute number and percentage of PD1-expressing CD8 + T cells in GL261 tumors at Day 21 (**A**, **B**) and Day 28 (**C**) post-implantation. **D**–**F** Fold change in absolute number and percentage of TIGIT-expressing CD8 + T cells in GL261 tumors at Day 21 (**D**, **E**) and Day 28 (**F**) post-implantation. **G**–**I** Fold change in absolute number and percentage of TIM3-expressing CD8 + T cells in GL261 tumors at Day 21 (**G**, **H**) and Day 28 (**I**) post-implantation. n = 12–16 per group. Day 21 panels: n = 7–16 per group. Data reported for 2 independent experiments. Day 28 panels: n = 6–8 per group. Data reported for 1 representative experiment

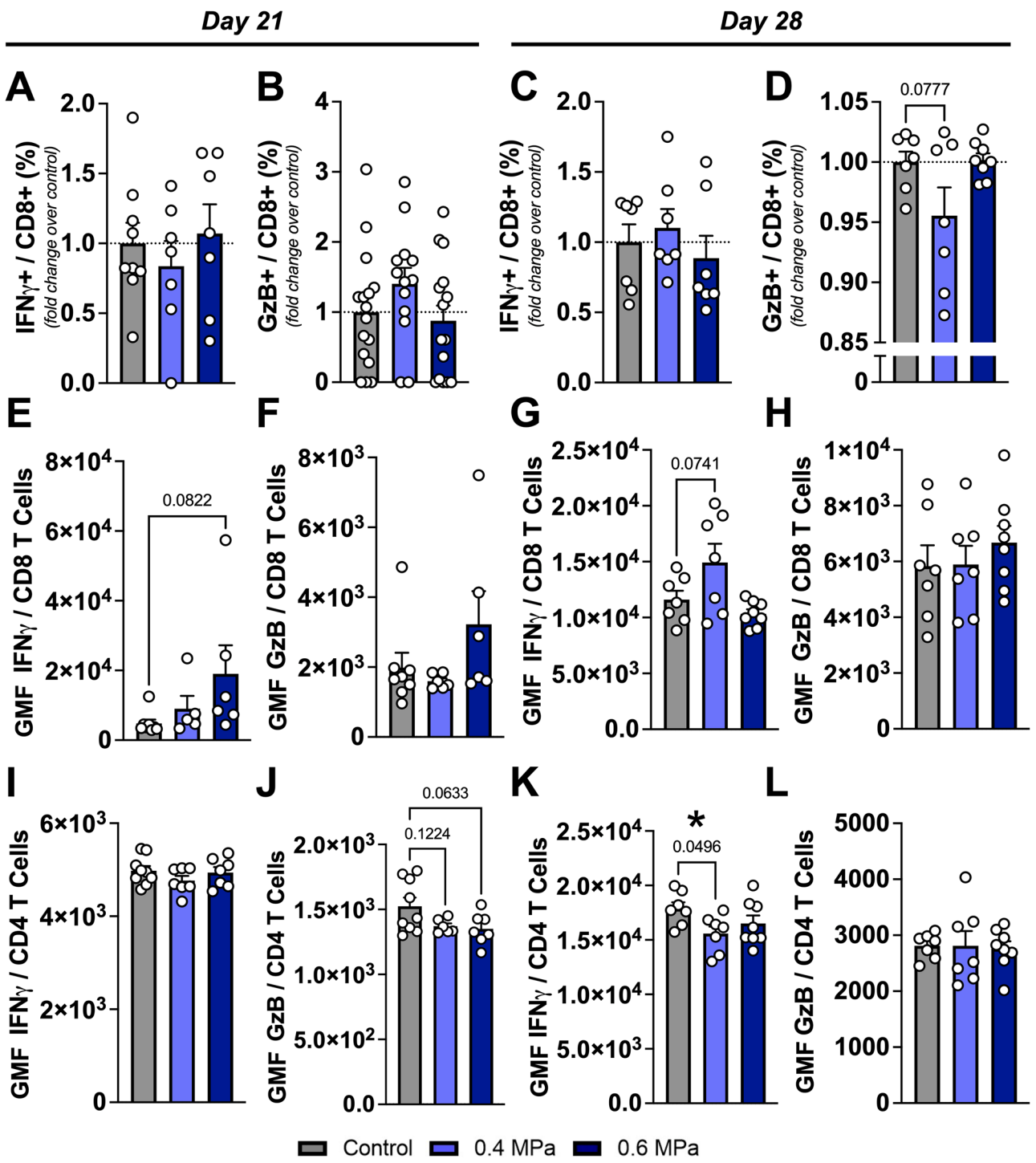

Fig. 5 Functional assessment of intratumoral T cells. **A**–**D** Fold change in percentage of CD8 + T cells expressing interferon-γ (IFN-γ) or granzyme-B (GzB) in GL261 tumors at Day 21 (**A**, **B**) and Day 28 (**C**, **D**) post-implantation. **E**–**H** Geometric fluorescence intensity (GMF) of IFN-γ or GzB on CD8 + T cells in GL261 tumors at Day 21 (**E**, **F**) and Day 28 (**G**, **H**) post-implantation. **I**–**L** GMF of IFN-γ or GzB on CD4 + T cells in GL261 tumors at Day 21 (**I**, **J**) and Day 28 (**K**, **L**) post-implantation. Data from one representative experiment reported in (**E**–**L**). Percentage panels: n = 7–16 per group. Data reported for 1–2 independent experiments. GMF panels: n = 5–9. Data reported for 1 representative experiment

Supplementary Information The online version contains supplementary material available at https://doi.org/10.1007/s11060-021-03887-4.

Acknowledgements The authors thank Dr. Sasha Klibanov (UVA) for supplying microbubbles for all FUS studies as well as Breanna Noffsinger (UVA) for her guidance and assistance with immunological characterization studies. Additional thanks to the UVA Carter Immunology Center for enabling generation of flow cytometry data.

Author contributions NDS and ARW designed and performed experiments and data analysis. NDS wrote the manuscript. WJG and GWM performed MR imaging and supported FUS studies. RJP and TNJB provided funding support, supervised all studies, and contributed to writing the manuscript. All authors reviewed and approved the manuscript.

Funding This study was supported by National Institutes of Health Grants R01EB030409 and R21NS118278 (R.J.P.) and R01CA197111 (R.J.P. and T.N.J.B.), the Focused Ultrasound Foundation (T.N.J.B. and R.J.P.), the Melanoma Research Alliance (Grant #: 348727) and the Schiff Foundation (T.N.J.B. and R.J.P.). N.D.S. was supported by the National Institutes of Health Director's Early Independence Award DP5 (DP5OD031846), National Cancer Institute F99/K00 Predoctoral to Postdoctoral Fellow Transition Award (F99CA234954 and K00CA234954), NSF Graduate Research Fellowship, and UVA School of Medicine Wagner Fellowship. A.R.W. was supported by an NIH Cancer Training Grant (2T32CA009109-41), the UVA Cancer Center Farrow Fellowship and NCI Cancer Center Support Grant P30 CA44579.

Data availability Data associated with this study are included in the main text or supplementary files for this article and are available from the corresponding author on reasonable request.

Code availability N/A.

Declarations

Conflict of interest The authors declare that they have no conflicts/competing interests.

Ethical approval Mouse protocols were approved by the IACUC committee at the University of Virginia (UVA).

Consent to participate N/A.

Consent for publication N/A.

References

1. Razavi S-M, Lee KE, Jin BE, Aujla PS, Gholamin S, Li G (2016) Immune evasion strategies of glioblastoma. Front Surg 3:11. https://doi.org/10.3389/fsurg.2016.00011
2. Fecci PE, Sampson JH (2019) The current state of immunotherapy for gliomas: an eye toward the future. J Neurosurg 131:657–666. https://doi.org/10.3171/2019.5.JNS181762
3. Louveau A, Smirnov I, Keyes TJ, Eccles JD, Sherin J, Peske JD, Derecki NC, Castle D, Mandell JW, Kevin L, Harris TH, Kipnis J (2016) Structural and functional features of central nervous system lymphatics. Nature 523:337–341. https://doi.org/10.1038/nature14432
4. Fecci PE, Heimberger AB, Sampson JH (2014) Immunotherapy for primary brain tumors: no longer a matter of privilege. Clin Cancer Res 20:5620–5629. https://doi.org/10.1158/1078-0432.CCR-14-0832
5. Antonios JP, Soto H, Everson RG, Orpilla J, Moughon D, Shin N, Sedighim S, Yong WH, Li G, Cloughesy TF (2016) PD-1 blockade enhances the vaccination-induced immune response in glioma. JCI insight 1:e87059. https://doi.org/10.1172/jci.insight.87059
6. Reardon DA, Gokhale PC, Klein SR, Ligon KL, Rodig SJ, Ramkissoon SH, Jones KL, Conway AS, Liao X, Zhou J, Wen PY, Van Den Abbeele AD, Hodi FS, Qin L, Kohl NE, Sharpe AH, Dranoff G, Freeman GJ (2016) Glioblastoma eradication following immune checkpoint blockade in an orthotopic, immunocompetent model. Cancer Immunol Res 4:124–135. https://doi.org/10.1158/2326-6066.CIR-15-0151
7. Prins RM, Wang X, Soto H, Young E, Lisiero DN, Fong B, Everson R, Yong WH, Lai A, Li G (2013) Comparison of glioma-associated antigen peptide-loaded versus autologous tumor lysate-loaded dendritic cell vaccination in malignant glioma patients. J Immunother 36:152. https://doi.org/10.1097/CJI.0b013e3182811ae4
8. Reardon DA, Wucherpfennig K, Chiocca EA (2017) Immunotherapy for glioblastoma: on the sidelines or in the game? Discov Med 24:201–208
9. Lim M, Xia Y, Bettegowda C, Weller M (2018) Current state of immunotherapy for glioblastoma. Nat Rev Clin Oncol 15:422–442. https://doi.org/10.1038/s41571-018-0003-5
10. Kovacs Z, Werner B, Rassi A, Sass JO, Martin-Fiori E, Bernasconi M (2014) Prolonged survival upon ultrasound-enhanced doxorubicin delivery in two syngenic glioblastoma mouse models. J Control Release 187:74–82. https://doi.org/10.1016/j.jconrel.2014.05.033
11. Aryal M, Vykhodtseva N, Zhang Y-Z, McDannold N (2015) Multiple sessions of liposomal doxorubicin delivery via focused ultrasound mediated blood-brain barrier disruption: a safety study. J Control Release 204:60–69. https://doi.org/10.1016/j.jconrel.2015.02.033
12. Arvanitis CD, Askoxylakis V, Guo Y, Datta M, Kloepper J, Ferraro GB, Bernabeu MO, Fukumura D, McDannold N, Jain RK (2018) Mechanisms of enhanced drug delivery in brain metastases with focused ultrasound-induced blood-tumor barrier disruption. Proc Natl Acad Sci USA 115:E8717–E8726. https://doi.org/10.1073/pnas.1807105115
13. Timbie KF, Afzal U, Date A, Zhang C, Miller GW, Suk JS, Hanes J, Price RJ (2017) MR image-guided delivery of cisplatin-loaded brain-penetrating nanoparticles to invasive glioma with focused ultrasound. J Control Release. https://doi.org/10.1016/j.jconrel.2017.03.017
14. Liu H-L, Hsu P-H, Lin C-Y, Huang C-W, Chai W-Y, Chu P-C, Huang C-Y, Chen P-Y, Yang L-Y, Kuo JS, Wei K-C (2016) Focused ultrasound enhances central nervous system delivery of bevacizumab for malignant glioma treatment. Radiology 281:99–108. https://doi.org/10.1227/NEU.0000000000001451
15. Park EJ, Zhang YZ, Vykhodtseva N, McDannold N (2012) Ultrasound-mediated blood-brain/blood-tumor barrier disruption improves outcomes with trastuzumab in a breast cancer brain metastasis model. J Control Release 163:277–284. https://doi.org/10.1016/j.jconrel.2012.09.007
16. Kobus T, Zervantonakis IK, Zhang Y, McDannold NJ (2016) Growth inhibition in a brain metastasis model by antibody delivery using focused ultrasound-mediated blood-brain barrier disruption. J Control Release 238:281–288. https://doi.org/10.1016/j.jconrel.2016.08.001

17. Kinoshita M, McDannold N, Jolesz FA, Hynynen K (2006) Noninvasive localized delivery of Herceptin to the mouse brain by MRI-guided focused ultrasound-induced blood-brain barrier disruption. Proc Natl Acad Sci USA 103:11719–11723. https://doi.org/10.1073/pnas.0604318103
18. Sheybani ND, Breza VR, Paul S, McCauley KS, Berr SS, Miller GW, Neumann KD, Price RJ (2021) ImmunoPET-informed sequence for focused ultrasound-targeted mCD47 blockade controls glioma. J Control Release. https://doi.org/10.1016/j.jconrel.2021.01.023
19. Chen P-Y, Hsieh H-Y, Huang C-Y, Lin C-Y, Wei K-C, Liu H-L (2015) Focused ultrasound-induced blood-brain barrier opening to enhance interleukin-12 delivery for brain tumor immunotherapy: a preclinical feasibility study. J Transl Med 13:93. https://doi.org/10.1186/s12967-015-0451-y
20. Alkins R, Burgess A, Ganguly M, Francia G, Kerbel R, Wels WS, Hynynen K (2013) Focused ultrasound delivers targeted immune cells to metastatic brain tumors. Cancer Res 73:1892–1899. https://doi.org/10.1158/0008-5472.CAN-12-2609
21. Alkins R, Burgess A, Kerbel R, Wels WS, Hynynen K (2016) Early treatment of HER2-amplified brain tumors with targeted NK-92 cells and focused ultrasound improves survival. Neuro Oncol 18:974–981. https://doi.org/10.1093/neuonc/nov318
22. Kovacs ZI, Kim S, Jikaria N, Qureshi F, Milo B, Lewis BK, Bresler M, Burks SR, Frank JA (2017) Disrupting the blood-brain barrier by focused ultrasound induces sterile inflammation. Proc Natl Acad Sci USA 114:E75–E84. https://doi.org/10.1073/pnas.1614777114
23. McMahon D, Bendayan R, Hynynen K (2017) Acute effects of focused ultrasound-induced increases in blood-brain barrier permeability on rat microvascular transcriptome. Sci Rep 7:45657. https://doi.org/10.1038/srep45657
24. McMahon D, Hynynen K (2018) Reply to Kovacs et al.: Concerning acute inflammatory response following focused ultrasound and microbubbles in the brain. Theranostics 8:2249–2250. https://doi.org/10.7150/thno.25468
25. Sinharay S, Tu T-W, Kovacs ZI, Schreiber-Stainthorp W, Sundby M, Zhang X, Papadakis GZ, Reid WC, Frank JA, Hammoud DA (2019) In vivo imaging of sterile microglial activation in rat brain after disrupting the blood-brain barrier with pulsed focused ultrasound: [18F]DPA-714 PET study. J Neuroinflamm 16:155. https://doi.org/10.1186/s12974-019-1543-z
26. Mathew AS, Gorick CM, Thim EA, Garrison WJ, Klibanov AL, Miller GW, Sheybani ND, Price RJ (2020) Transcriptomic response of brain tissue to focused ultrasound-mediated blood–brain barrier disruption depends strongly on anesthesia. Bioeng Transl Med 6:e10198. https://doi.org/10.1002/btm2.10198
27. Curley CT, Sheybani ND, Bullock TN, Price RJ (2017) Focused ultrasound immunotherapy for central nervous system pathologies: challenges and opportunities. Theranostics 7:3608–3623. https://doi.org/10.7150/thno.21225
28. Curley CT, Stevens AD, Mathew AS, Stasiak K, Garrison WJ, Miller GW, Sheybani ND, Engelhard VH, Bullock TNJ, Price RJ (2020) Immunomodulation of intracranial melanoma in response to blood-tumor barrier opening with focused ultrasound. Theranostics 10:8821–8833. https://doi.org/10.7150/thno.47983
29. Kovacs ZI, Tu T-W, Sundby M, Qureshi F, Lewis BK, Jikaria N, Burks SR, Frank JA (2018) MRI and histological evaluation of pulsed focused ultrasound and microbubbles treatment effects in the brain. Theranostics 8:4837–4855. https://doi.org/10.7150/thno.24512
30. McDannold N, Zhang Y, Vykhodtseva N (2017) The effects of oxygen on ultrasound-induced blood-brain barrier disruption in mice. Ultrasound Med Biol 43:469–475. https://doi.org/10.1016/j.ultrasmedbio.2016.09.019
31. McDannold N, Zhang Y, Vykhodtseva N (2011) Blood-brain barrier disruption and vascular damage induced by ultrasound bursts combined with microbubbles can be influenced by choice of anesthesia protocol. Ultrasound Med Biol 37:1259–1270. https://doi.org/10.1016/j.ultrasmedbio.2011.04.019
32. Sabbagh A, Beccaria K, Ling X, Marisetty A, Ott M, Caruso H, Barton E, Kong L-Y, Fang D, Latha K, Zhang DY, Wei J, DeGroot J, Curran MA, Rao G, Hu J, Desseaux C, Bouchoux G, Canney M, Carpentier A, Heimberger AB (2021) Opening of the blood-brain barrier using low-intensity pulsed ultrasound enhances responses to immunotherapy in preclinical glioma models. Clin Cancer Res 27:4325–4337. https://doi.org/10.1158/1078-0432.CCR-20-3760
33. Idbaih A, Canney M, Belin L, Desseaux C, Vignot A, Bouchoux G, Asquier N, Law-Ye B, Leclercq D, Bissery A, De Rycke Y, Trosch C, Capelle L, Sanson M, Hoang-Xuan K, Dehais C, Houillier C, Laigle-Donadey F, Mathon B, André A, Lafon C, Chapelon J, Delattre J, Carpentier A (2019) Safety and feasibility of repeated and transient blood-brain barrier disruption by pulsed ultrasound in patients with recurrent glioblastoma. Clin Cancer Res. https://doi.org/10.1158/1078-0432.CCR-18-3643
34. Carpentier A, Canney M, Vignot A, Reina V, Beccaria K, Horodyckid C, Karachi C, Leclercq D, Lafon C, Chapelon J-Y, Capelle L, Cornu P, Sanson M, Hoang-Xuan K, Delattre J-Y, Idbaih A (2016) Clinical trial of blood-brain barrier disruption by pulsed ultrasound. Sci Transl Med 8:343re2. https://doi.org/10.1126/scitranslmed.aaf6086
35. Mainprize T, Lipsman N, Huang Y, Meng Y, Bethune A, Ironside S, Heyn C, Alkins R, Trudeau M, Sahgal A, Perry J, Hynynen K (2019) Blood-brain barrier opening in primary brain tumors with non-invasive MR-guided focused ultrasound: a clinical safety and feasibility study. Sci Rep 9:321. https://doi.org/10.1038/s41598-018-36340-0
36. Abrahao A, Meng Y, Llinas M, Huang Y, Hamani C, Mainprize T, Aubert I, Heyn C, Black SE, Hynynen K, Lipsman N, Zinman L (2019) First-in-human trial of blood-brain barrier opening in amyotrophic lateral sclerosis using MR-guided focused ultrasound. Nat Commun 10:4373. https://doi.org/10.1038/s41467-019-12426-9
37. Lipsman N, Meng Y, Bethune AJ, Huang Y, Lam B, Masellis M, Herrmann N, Heyn C, Aubert I, Boutet A, Smith GS, Hynynen K, Black SE (2018) Blood–brain barrier opening in Alzheimer's disease using MR-guided focused ultrasound. Nat Commun 9:2336. https://doi.org/10.1038/s41467-018-04529-6
38. Rezai AR, Ranjan M, D'Haese P-F, Haut MW, Carpenter J, Najib U, Mehta RI, Chazen JL, Zibly Z, Yates JR, Hodder SL, Kaplitt M (2020) Noninvasive hippocampal blood-brain barrier opening in Alzheimer's disease with focused ultrasound. Proc Natl Acad Sci USA 117:9180–9182. https://doi.org/10.1073/pnas.2002571117
39. Mead BP, Kim N, Miller GW, Hodges D, Mastorakos P, Klibanov AL, Mandell JW, Hirsh J, Suk JS, Hanes J, Price RJ (2017) novel focused ultrasound gene therapy approach noninvasively restores dopaminergic neuron function in a rat Parkinson's disease model. Nano Lett 17:3533–3542. https://doi.org/10.1021/acs.nanolett.7b00616
40. Burke CW, Suk JS, Kim AJ, Hsiang Y-HJ, Klibanov AL, Hanes J, Price RJ (2012) Markedly enhanced skeletal muscle transfection achieved by the ultrasound-targeted delivery of non-viral gene nanocarriers with microbubbles. J Control Release 162:414–421. https://doi.org/10.1016/j.jconrel.2012.07.005
41. Kovacs ZI, Kim S, Jikaria N, Qureshi F, Milo B, Lewis BK, Bresler M, Burks SR, Frank JA (2016) Disrupting the blood–brain barrier by focused ultrasound induces sterile inflammation. Proc Natl Acad Sci USA 114:E75–E84. https://doi.org/10.1073/pnas.1614777114
42. McMahon D, Hynynen K (2017) Acute inflammatory response following increased blood-brain barrier permeability induced by

focused ultrasound is dependent on microbubble dose. Theranostics 7:3989–4000. https://doi.org/10.7150/thno.21630
43. Bing C, Hong Y, Hernandez C, Rich M, Cheng B, Munaweera I, Szczepanski D, Xi Y, Bolding M, Exner A, Chopra R (2018) Characterization of different bubble formulations for blood-brain barrier opening using a focused ultrasound system with acoustic feedback control. Sci Rep 8:7986. https://doi.org/10.1038/s41598-018-26330-7
44. Wu S-K, Chu P-C, Chai W-Y, Kang S-T, Tsai C-H, Fan C-H, Yeh C-K, Liu H-L (2017) Characterization of different microbubbles in assisting focused ultrasound-induced blood-brain barrier opening. Sci Rep 7:46689. https://doi.org/10.1038/srep46689
45. McDannold N, Vykhodtseva N, Hynynen K (2007) Use of ultrasound pulses combined with Definity for targeted blood-brain barrier disruption: a feasibility study. Ultrasound Med Biol 33:584–590. https://doi.org/10.1016/j.ultrasmedbio.2006.10.004
46. Curley CT, Mead BP, Negron K, Garrison WJ, Miller GW, Kingsmore KM, Thim EA, Song J, Munson JM, Klibanov AL, Suk JS, Hanes J, Price RJ (2020) Augmentation of brain tumor interstitial flow via focused ultrasound promotes brain-penetrating nanoparticle dispersion and transfection. Sci Adv 6:aay1344. https://doi.org/10.1126/sciadv.aay1344
47. Palucka AK, Ueno H, Fay J, Banchereau J (2008) Dendritic cells: a critical player in cancer therapy? J Immunother 31:793–805. https://doi.org/10.1097/CJI.0b013e31818403bc
48. Mellman I (2013) Dendritic cells: master regulators of the immune response. Cancer Immunol Res 1:145–149. https://doi.org/10.1158/2326-6066.CIR-13-0102
49. Barkauskas DS, Dorand RD, Myers JT, Evans TA, Barkauskas KJ, Askew D, Purgert R, Huang AY (2015) Focal transient CNS vessel leak provides a tissue niche for sequential immune cell accumulation during the asymptomatic phase of EAE induction. Exp Neurol 266:74–85. https://doi.org/10.1016/j.expneurol.2015.02.018
50. Karman J, Ling C, Sandor M, Fabry Z (2004) Initiation of immune responses in brain is promoted by local dendritic cells. J Immunol 173:2353–2361. https://doi.org/10.4049/jimmunol.173.4.2353
51. Ling C, Sandor M, Fabry Z (2003) In situ processing and distribution of intracerebrally injected OVA in the CNS. J Neuroimmunol 141:90–98. https://doi.org/10.1016/s0165-5728(03)00249-2
52. Chen S, Crabill GA, Pritchard TS, McMiller TL, Wei P, Pardoll DM, Pan F, Topalian SL (2019) Mechanisms regulating PD-L1 expression on tumor and immune cells. J Immunother Cancer 7:305. https://doi.org/10.1186/s40425-019-0770-2
53. Gao J, Zheng Q, Xin N, Wang W, Zhao C (2017) CD155, an onco-immunologic molecule in human tumors. Cancer Sci 108:1934–1938. https://doi.org/10.1111/cas.13324
54. Liu F, Huang J, Xiong Y, Li S, Liu Z (2019) Large-scale analysis reveals the specific clinical and immune features of CD155 in glioma. Aging (Albany NY) 11:5463. https://doi.org/10.18632/aging.102131
55. Hung AL, Maxwell R, Theodros D, Belcaid Z, Mathios D, Luksik AS, Kim E, Wu A, Xia Y, Garzon-Muvdi T (2018) TIGIT and PD-1 dual checkpoint blockade enhances antitumor immunity and survival in GBM. Oncoimmunology 7:e1466769. https://doi.org/10.1080/2162402X.2018.1466769